



HAL
open science

El-Numodis: a new tool to model dislocation and surface interactions

Javier Antonio Gonzalez Joa, Laurent Dupuy, Peter Råback, Marc Fivel,
Michel Perez, Jonathan Amodeo

► **To cite this version:**

Javier Antonio Gonzalez Joa, Laurent Dupuy, Peter Råback, Marc Fivel, Michel Perez, et al.. El-Numodis: a new tool to model dislocation and surface interactions. *Modelling and Simulation in Materials Science and Engineering*, 2023, 31 (5), pp.055003. 10.1088/1361-651X/acd01b . hal-04098676

HAL Id: hal-04098676

<https://hal.science/hal-04098676>

Submitted on 16 May 2023

HAL is a multi-disciplinary open access archive for the deposit and dissemination of scientific research documents, whether they are published or not. The documents may come from teaching and research institutions in France or abroad, or from public or private research centers.

L'archive ouverte pluridisciplinaire **HAL**, est destinée au dépôt et à la diffusion de documents scientifiques de niveau recherche, publiés ou non, émanant des établissements d'enseignement et de recherche français ou étrangers, des laboratoires publics ou privés.

Originally published in Modelling and Simulation in Materials Science and Engineering, May 16th 2023. Cite as: Gonzalez Joa *et al.* Modelling Simul. Mater. Sci. Eng. 31 (2023) 055003 (22pp)

El-Numodis: a new tool to model dislocation and surface interactions

Javier Antonio Gonzalez Joa

Univ Lyon, INSA Lyon, UCBL, MATEIS, UMR5510, 69621 Villeurbanne, France

Laurent Dupuy

DES-Service de Recherches Métallurgiques Appliquées, CEA, Université Paris-Saclay, F-91191 Gif sur Yvette, France

Peter Råback

CSC - IT Center for Science, Box 405, 02101 Espoo, Finland

Marc Fivel

Univ. Grenoble Alpes, Grenoble-INP, CNRS, SIMaP, F-38402 Grenoble, France

Michel Perez

Univ Lyon, INSA Lyon, UCBL, MATEIS, UMR5510, 69621 Villeurbanne, France

Jonathan Amodeo*

Univ Lyon, CNRS, INSA Lyon, UCBL, MATEIS, UMR5510, 69621 Villeurbanne, France

Aix-Marseille Univ, Université de Toulon, CNRS, IM2NP, Marseille, France

E-mail: jonathan.amodeo@cnrs.fr

Abstract.

While surfaces are known to have a limited impact on the mechanical properties of crystalline materials at the macroscopic scale, they play a key role at small-scale behaving alternatively as sources or sinks of various plastic deformation processes. In this study, we present a new tool called El-Numodis that relies on the superposition method to couple the discrete dislocation dynamics code Numodis to Elmer, an open-source finite-element-modeling tool. After few years of development, El-Numodis allows now for the simulation of small-scale object deformation and mechanical properties based on a large set of surface-related processes including stress-free boundaries, mirrored dislocations and a Monte-Carlo based dislocation nucleation mechanism. Here we present the main features of the code as well as numerical test-cases and benchmarks going from classical boundary value problems to tensile tests on model thin film.

Indeed, *nanotech* is now an important segment of the modern material industry. The wide range of applications of nanodevices is mainly due to the advantages brought by the radical change of their properties (mechanical, surface, optical, chemical, *etc.*) induced by their size, compared to bulk materials. As examples, nanowires are employed for digital data storage due to their superparamagnetic capability that relies on a very fast response to external fields with almost zero remanence [13, 14], nanoparticles are also currently used to improve the performance of lubricants [15, 16] or as compounds to build implants due to their high-strength and wear resistance [17]. Overall, nanocrystals and their outstanding mechanical properties (*smaller is stronger*) are now widely used to improve bulk materials [18, 19] and their strength *vs.* size dependence mostly arises from the increase of the surface over volume ratio when scaling down the sample size [20, 21].

While the flow of bulk materials is known to be governed by a dislocation multiplication process from an existing defective microstructure, the plastic deformation of nano-objects is controlled by a Surface Dislocation Nucleation (SDN) mechanism that requires a much larger stress than in the classical dislocation multiplication case (stress increased by a factor of 10 to 1000) [22–25]. In fact, nanocrystals are known to be dislocation-scarce (or free) due to both the soft fabrication routes from which they are derived (*e.g.*, crystal growth, dewetting, lithography) as well as to surface-induced image forces [26, 27] that pump the dislocation density out, this latter being intrinsically concomitant to the aforementioned SDN process.

Several experimental and numerical methods currently exist to try to understand the mechanical behaviour of nano-objects. For example, nanocompression in the Scanning or Transmission Electron Microscope (SEM or TEM) are the most used experimental techniques in the field [28–30]. Experiments are reported for sample sizes ranging from several micrometers down to few tens nanometers as well as for low deformation rate (10^{-4} to ~ 1 s $^{-1}$). While the use of TEM allows for microstructure, defect and surface characterizations at the nanoscale, it is still a complex and expensive method and several issues including sample misalignment, contamination or oxidation are commonly reported [31–33]. Thus, computational methods are often used to support the interpretation of nanomechanics experiments. On one hand, MD is the most used numerical technique to simulate the mechanical properties of nano-objects as relying on the description of atomic-scale processes [21, 34]. It is based on interatomic potentials used to compute atomic forces and integrate the dynamics of molecular systems *e.g.*, in a sample under load when applied to the field of nanomechanics. However, MD sample size is usually limited to few tens of nanometers while nano-objects can be of few hundreds and, furthermore, MD is performed at particularly high strain-rate ($\sim 10^8$ s $^{-1}$) due to prohibitive computational costs.

On the other hand, while DDD allows for larger sample size and strain rates both being closer to experimental conditions, it also has some drawbacks. Indeed, DDD allows to model dislocations on the basis of constitutive equations rather than atomic interactions

what makes the model less expensive in terms of cpu costs but has the disadvantage of being less accurate. Furthermore, DDD codes are generally developed for bulk applications and often miss nanoscale features. The major lack relies on the elastic theory the DDD is based on that usually assumes an infinite continuum. This peculiarity raises the issue of finite Boundary Conditions (BCs) as DDD was originally developed to tackle configurations close to bulk conditions *i.e.*, using Periodic Boundary Conditions (PBCs) or free-BCs, without explicitly considering realistic surfaces. In addition, former DDD codes (*e.g.*, microMegas [35,36], Paradis [37], Tridis [2,38]) have not been originally developed to describe dislocation nucleation processes. While this latter is not crucial to simulate bulk mechanics, it is imperative to model nanoscale mechanical properties due to the aforementioned SDN process. In this context, the development of quantitative numerical tools to investigate the mechanical properties of small-scale objects including the effect of surfaces, sample size, strain rate as well as the ability to account for most of nanoscale elementary deformation processes emerges as a crucial step up to improve our understanding of micro and nanomechanics [33].

Boundary Value Problems (BVPs) related to surfaces or interfaces can be addressed coupling the DDD with the Finite-Element Method (FEM) using various kinds of approaches such as the SuperPosition Method (SPM) that relies on a linear stress correction originally proposed by Van der Giessen and Needleman [39], the Discrete Continuous Method (DCM) proposed by Devincre and collaborators [40–42] based on the eigenstrain formalism of Mura [43] or the Fast Fourier Transform (FFT) dislocation approach which is increasingly used by the community [44,45]. As an example of application, a DCM-FFT approach was recently used by Kohnert and colleagues to quantify the effect of surfaces and TEM lamella thinning on the dislocation density [46].

Here we present our approach called El-Numodis which is based on the SPM and integrate specific features adapted to nanomechanical simulations. El-Numodis relies on the coupling of the DDD code Numodis [47,48] and the open-source FEM software Elmer [49]. It benefits of a particularly accurate and parallel nodal DDD framework that integrates top of the art features such as various implementations of the elastic theory, the singular and non-singular theories for dislocations [26,50] as well as additional ingredients to better model deformation tests at small-scales accounting for surface effects as *e.g.*, the Weygand’s approach for dislocation *vs.* surface interactions [27] and a Monte-Carlo routine for homogeneous and heterogeneous dislocation nucleation, as inferred from the harmonic Transition State Theory (TST) [51].

In the following, we start with a brief reminder about the DDD and FEM techniques in the context of the parent codes Numodis and Elmer, then, the main aspects of the coupling are introduced (SPM basics, coupling and interfacing procedures, dislocation nucleation and interaction with surfaces, *etc.*). Finally, an extended last section composed of various validation tests and applications complete the study.

2. Numerical methods

2.1. Basics on DDD and FEM: methodologies and parent codes

The DDD is a mesoscopic approach developed to investigate the collective behaviour of dislocations. This method was originally developed in the late 80' to study the evolution of a dislocation population under load in metals [52]. Since, it was further used to investigate various issues including strain hardening (see *e.g.*, [3,53]), irradiation defects [48, 54, 55], fatigue [56, 57] or nanoindentation [58] in metals. Few applications in oxides and minerals can also be found [12, 59–61]. General details about the DDD method can be found in Refs. [36, 62, 63].

Numodis is a versatile DDD code developed by the french Atomic Energy Center (CEA) used here in the DDD/FEM coupling framework of El-Numodis. Up to now, Numodis has shown to be particularly suited to investigate the influence of radiation-induced defects on the plastic behavior of metals such as iron [48, 64] or zirconium alloys [47] with one-to-one cross-validations of the DDD outcomes against MD and experiments. From a technical point of view, Numodis is a C++ nodal code in which dislocations are described by nodes interconnected into segments characterized by their Burgers vector and glide plane. It can be used either serial or parallel using the openMP protocol. In Numodis, a remeshing algorithm ensures that each segment length respects an admissible size range chosen in accordance with the characteristic size of the investigated phenomenon. The force acting on the nodes is computed within the singular [26] or non-singular [65] dislocation theoretical framework using the analytical formulation derived by Arsenlis *et al.* [37]. Additional dislocation core forces can be accounted using core energy terms [66–68]. The velocity of each node is computed using a classical variational approach [27, 65] assuming an overdamped motion and various kind of dedicated mobility laws including *e.g.*, viscous or thermally-activated glide assigned on each segment character and slip system. Dislocation contact reactions (junction, annihilation, crossed-states, *etc.*) are computed using the elastic theory allowing to model the dislocation microstructure evolution and strain hardening. The methodology used in El-Numodis is inspired from the seminal work of Bulatov and collaborators [37, 69] and can be resumed as follow. A collision detection algorithm is used at each timestep to predict incoming dislocation contact reactions with other dislocations or microstructural defects such as grain boundaries or precipitates. When a collision is detected, a new node is generated at the contact point and is kept fixed during the current DDD time step allowing for the rest of the dislocation microstructure to relax. If the collision is confirmed, the node evolves at step $n + 1$ depending on the situation while minimizing the energy using a split node algorithm. For example, for a contact between two dislocations, the node can split into two subsequent nodes forming a junction segment. At each time step, the code checks whether or not a node has to be split, a splittable node being defined as connected at least to three other nodes and must not be arbitrary pinned (*e.g.*, Frank-Read source).

Used in the El-Numodis context as an elastic solver, Elmer is a multiphysical FEM code written in modern Fortran that includes a large set of continuum-based physical models [49]. Up to now, Elmer was used in various fields of application to model *e.g.*, crystal growth [70], blood flow in elastic arteries [71], computational glaciology [72] or electrical machines [73]. Elmer uses high-level abstraction when treating individual equations for solving multiphysical problems and benefits from a modular structure and generic strategies that are useful when coupling it with other codes as *e.g.*, with OpenFOAM [74]. In the following, Elmer is coupled to Numodis using the SPM method [39, 75]. The Elmer physical model used for this coupling is the elasticity equation that can be solved using various types of 2D (triangular, quadrilateral) and 3D (tetrahedron, hexahedron, prism or wedge) elements. Finally, the linear system is solved using number of different direct (Umfpack, MUMPS and Pardiso packages) or iterative (conjugate gradient, basic preconditioning, Krylov subspace methods, *etc.*) techniques. Also, Elmer is interfaced with Hypre that provides an additional set of iterative solvers and preconditioners [76]. Finally, efficient octree-based interpolation methods that can be performed on nodes or on integration points are available for mapping results between computational meshes.

2.2. The superposition method and El-Numodis

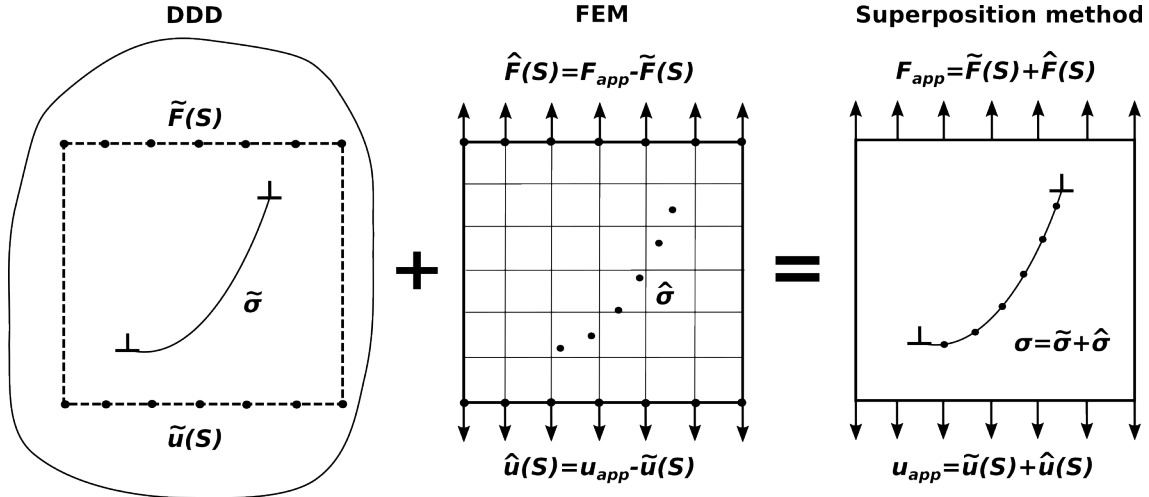


Figure 1: The superposition method. The stress field σ inside a finite-size volume containing dislocations (right-hand side) is obtained adding the dislocation self-stress $\tilde{\sigma}$ as computed by the DDD to the elastic stress $\hat{\sigma}$ as inferred from a FEM boundary corrected problem (left-hand side).

2.2.1. Introduction to the superposition method

The SPM method was first introduced by Needleman and collaborators to solve BVP problems [39]. It is based on the correction of the dislocation self-stress $\tilde{\sigma}$

and displacement fields $\tilde{\mathbf{u}}$ originally computed by a DDD code (assuming an infinite medium) at physical boundaries S using a FEM elastic solver. Assuming a finite-size volume, the SPM aims at imposing an applied force or displacement (\mathbf{F}_{app} and \mathbf{u}_{app} , respectively) via the BCs that is corrected by an homologous contribution ($\tilde{\boldsymbol{\sigma}}$ or $\tilde{\mathbf{u}}$) induced by a dislocation population as computed by the DDD using an infinite medium hypothesis (see Figure 1). For that purpose, the dislocation stress field computed at the boundary $\tilde{\boldsymbol{\sigma}}(\mathbf{S})$ is converted into forces $\tilde{\mathbf{F}}(\mathbf{S})$ using an appropriate conversion scheme when accounting for Neumann applied force BCs whereas applied displacement (Dirichlet) BCs $\tilde{\mathbf{u}}(\mathbf{S})$ are computed using the Barnett approach [77]. After solving the BVP, the field corrections ($\hat{\boldsymbol{\sigma}}$ or $\hat{\mathbf{u}}$) is added to the original internal fields ($\tilde{\boldsymbol{\sigma}}$ or $\tilde{\mathbf{u}}$) computed by the DDD what leads to the total stress $\boldsymbol{\sigma}$ or displacement fields \mathbf{u} (Equation 1). The FEM correction is computed at the dislocation Gauss points using a classical interpolation method and is further added to the dislocation stress or displacement field contribution. Thus, SPM allows for the mesoscale modeling of a finite-size domain including surfaces and interfaces (in the contrary to the self-standing DDD). This method that allows for arbitrary BCs was already used for various modeling applications such as nanoindentation [2,78], thin film [79] or micropillar compression [80] simulations.

$$\begin{aligned}\boldsymbol{\sigma} &= \tilde{\boldsymbol{\sigma}} + \hat{\boldsymbol{\sigma}} \\ \mathbf{u} &= \tilde{\mathbf{u}} + \hat{\mathbf{u}}\end{aligned}\tag{1}$$

2.3. El-Numodis operation

In the coupling approach, the FEM code Elmer drives the simulation and refers to the DDD as an external library. Number and format conversion drivers have been implemented for direct data transfer between the two codes while Elmer external solvers were upgraded here to manage the newly coupled BCs. In a nutshell, the coupling consists in three external routines and several Numodis functions being called as shown in Figure 2. The El-Numodis workflow can be described as follows:

- (i) *Loading deformation conditions.* El-Numodis requires a 3D geometrical mesh as well as a parameter file that are loaded at first. Among others, the parameters file contains the definition of the faces where the BCs (Dirichlet or Neumann) are applied, the total number of time steps, the output saving frequency, material elastic properties as well as the elastic solver parameters. At the end of this first step, Numodis is called using a first driver referred as *El-Numodis export bnodes*.
- (ii) *Calculation of $\tilde{\boldsymbol{\sigma}}(\mathbf{S})$ and $\tilde{\mathbf{u}}(\mathbf{S})$.* Specific DDD inputs as *e.g.*, the dislocation density distribution, are loaded by Numodis. Elmer associates parts of or all the surface nodes to specific BCs *i.e.*, Neumann (including traction-free nodes) or Dirichlet

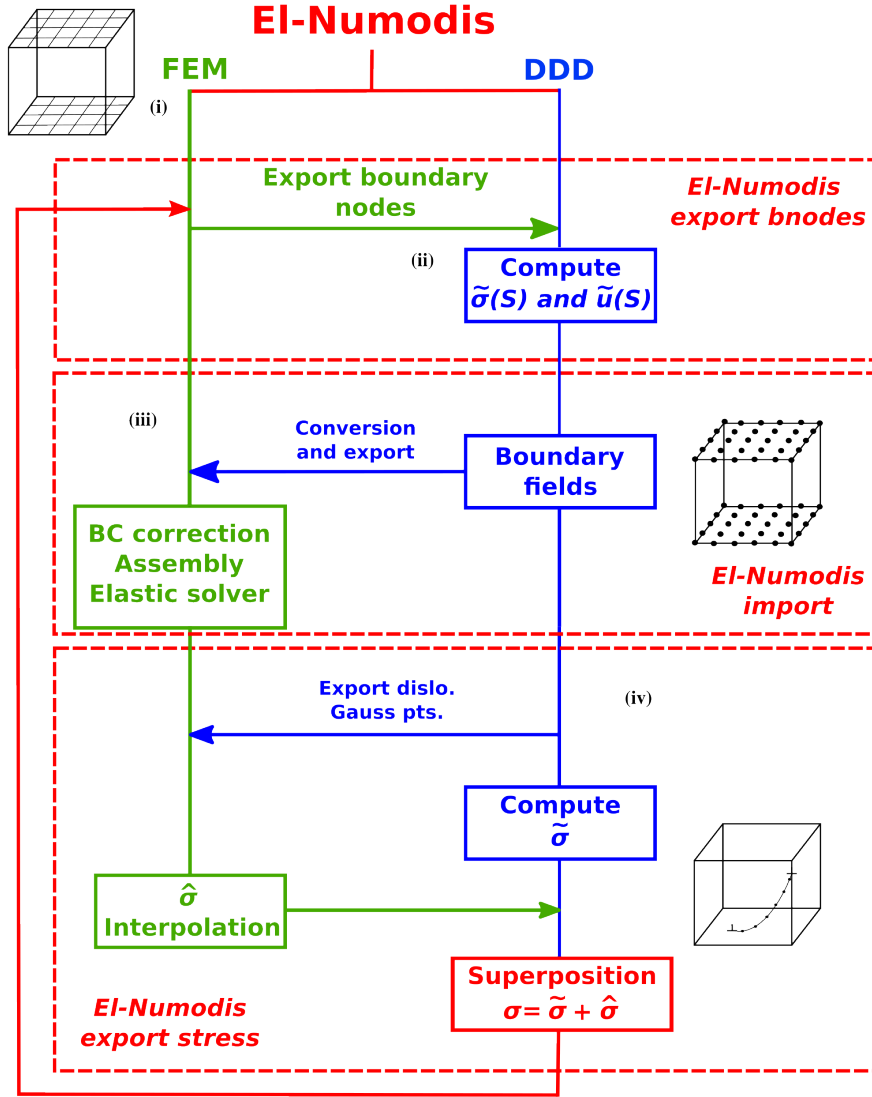


Figure 2: El-Numodis workflow. The FEM code Elmer masters the coupling using the DDD Numodis code as a library. Both contributions are illustrated in green and blue, respectively. The three main drivers of El-Numodis *i.e.*, *El-Numodis export Bnodes*, *El-Numodis import* and *El-Numodis export stress* are illustrated using red blocks. (i), (ii), (iii) and (iv) refer to the main operations as described in the text.

BCs. Then, the DDD computes the displacement and stress fields associated with the current dislocation density $\tilde{\sigma}(\mathbf{S})$ and $\tilde{\mathbf{u}}(\mathbf{S})$ at the specified BC nodes.

- (iii) *Fields regularisation.* A second driver called *El-Numodis import* converts $\tilde{\sigma}(\mathbf{S})$ into $\tilde{\mathbf{F}}(\mathbf{S})$ at Neumann boundary nodes and $\hat{\mathbf{F}}(\mathbf{S}) = \mathbf{F}_{app} - \tilde{\mathbf{F}}(\mathbf{S})$ as well as $\hat{\mathbf{u}}(\mathbf{S}) = \mathbf{u}_{app} - \tilde{\mathbf{u}}(\mathbf{S})$ are computed. Then, the assembly is performed accounting for a feedback loop to either adapt the applied stress or displacement. Finally, the linear elastic solver of Elmer computes $\hat{\sigma}$ everywhere inside the simulation volume.

- (iv) *Fields superposition.* Finally, the last driver *El-Numodis export stress* is called. It first lists dislocation Gauss points and then interpolates $\hat{\boldsymbol{\sigma}}$. The stress superposition as described by Equation 1 is performed leading to the effective stress state $\boldsymbol{\sigma}$. Then, a new DDD step is performed including force computation, possible nucleation event or dislocation displacement. The whole process is repeated up to the total amount of simulation time steps.

2.4. Field conversion and interpolation

By definition, stress and force are connected by a geometrical area. In FEM, the conversion from stress to force is performed retrieving stress values at the Gauss points of mesh elements and converting them into nodal values using the pseudo-inverse of a shape function associated to each mesh type. Figure 3a shows a typical example about how this is implemented in El-Numodis, associated here to a regular mesh of 8-nodes hexahedron elements for the sake of simplicity. As shown in Figure 3a, $\tilde{\boldsymbol{\sigma}}(\mathbf{S})$ is computed at the mesh nodes and the conversion from $\tilde{\boldsymbol{\sigma}}(\mathbf{S})$ to $\tilde{\mathbf{F}}(\mathbf{S})$ is done using a weighted area of normal vector \mathbf{n} associated to each node using Equation 2. The weighted area depends on the element shape and localization. Here, internal surface nodes are characterised by $A=1$ whereas corners and external edge nodes have associated area of $A/4$ and $A/2$, respectively.

$$\tilde{\mathbf{F}}(\mathbf{S}) = A\tilde{\boldsymbol{\sigma}}(\mathbf{S})\mathbf{n} \quad (2)$$

The stress at the dislocation Gauss points $\hat{\boldsymbol{\sigma}}_{gp}$ is derived from the FEM solution $\hat{\boldsymbol{\sigma}}$ originally computed at the mesh nodes. To interpolate and retrieve the solution at the dislocation Gauss point, it is necessary to (i) identify the element and the k nodes enclosing the respective dislocation Gauss point, (ii) transform the global coordinates (x,y,z) of the element nodes into a reference frame (ξ,η,ζ) (Figure 3b) and (iii) apply the shape function N_k . In the square mesh case depicted in Figure 3a, N_k and $\hat{\boldsymbol{\sigma}}_{gp}$ are provided by,

$$N_k = \frac{1}{8}(1 + \xi_{gp}\xi_k)(1 + \eta_{gp}\eta_k)(1 + \zeta_{gp}\zeta_k) \quad (3)$$

$$\hat{\boldsymbol{\sigma}}_{gp} = \sum_{k=1}^8 N_k \hat{\boldsymbol{\sigma}}_k \quad (4)$$

where k refers to nodes index. This method is commonly used in El-Numodis that benefits of various additional interpolation schemes (via Elmer) that could be adapted to the calculation of $\hat{\boldsymbol{\sigma}}_{gp}$. See *e.g.*, [81] for more details on field conversion and interpolation.

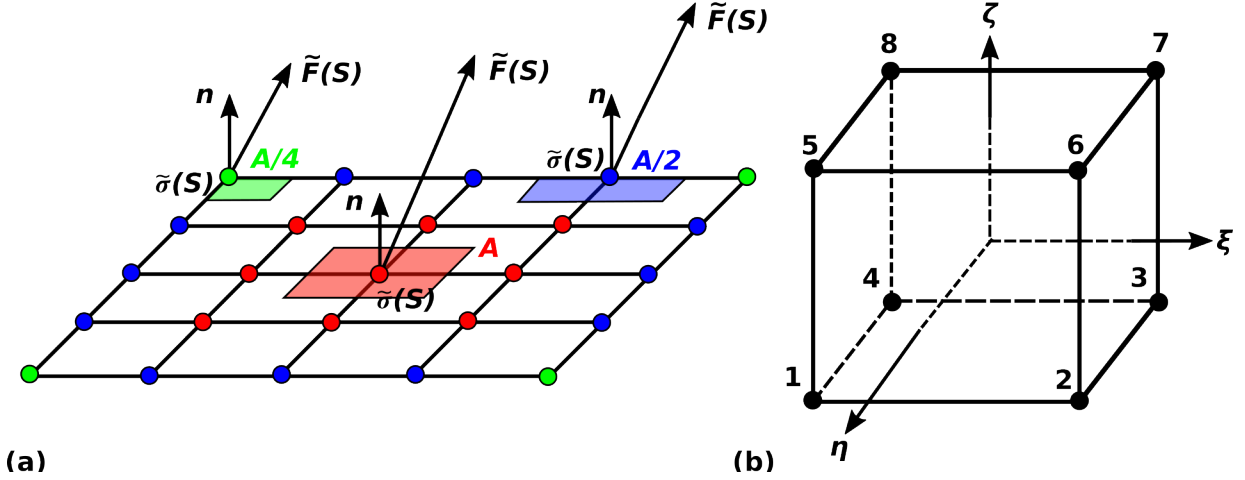


Figure 3: El-Numodis interpolation scheme using shape functions and fields conversion. (a) Representation of a surface mesh where stresses are converted into forces at the element nodes. Nodes and surface colors refer to respective types (green=corner, blue=side edge and red=internal). (b) The global coordinates (x,y,z) of each node is transformed into reference coordinate (ξ,η,ζ) with the new axes located at the center of the hexahedron element.

2.5. Dislocation and surfaces

El-Numodis is designed to model dislocations interacting with surfaces (optionally) using the mirror dislocation concept [26,27] to assist the FEM in field corrections. Indeed, when a dislocation approaches a surface, the local stress and displacement fields can be obtained adding the contribution of an *out-of-the-box* mirror dislocation to the original dislocation fields. While the field calculation will be discussed later, the topological aspects of the mirroring process in El-Numodis can be described as follow. First, following the seminal work of Weygand *et al.* [27], a dislocation close to a sample surface by a cutoff distance r_c^{im} is automatically replicated on the other side of the surface using planar symmetry as shown in Figure 4. The resulting mirror dislocation is characterized by a line with symmetric orientation but an opposite Burgers vector direction. While the mirror dislocation stress and displacement fields are accounted within the simulation cell in order to reduce image contributions, the image dislocation does not produce any plastic shear. If the dislocation is about to contact with the surface, the Numodis collision detection algorithm is used to identify dislocation segments about to react with their mirrored counterpart, both emerging at the surface. In this case, the dislocation contact reaction leads to the annihilation of both dislocations. Finally, the dislocation annihilated portion at the surface is replaced by a ledge made of surface nodes (Figure 4). The surface nodes have the same mobility as the bulk ones but are constrained to move only on the sample surface (with the possibility to pass from one surface to an other). Also, ledges benefit from the same properties as dislocations *i.e.*, they can superimpose or annihilate when several dislocations escape from the same surface but

do not produce any stress or displacement field inside the sample.

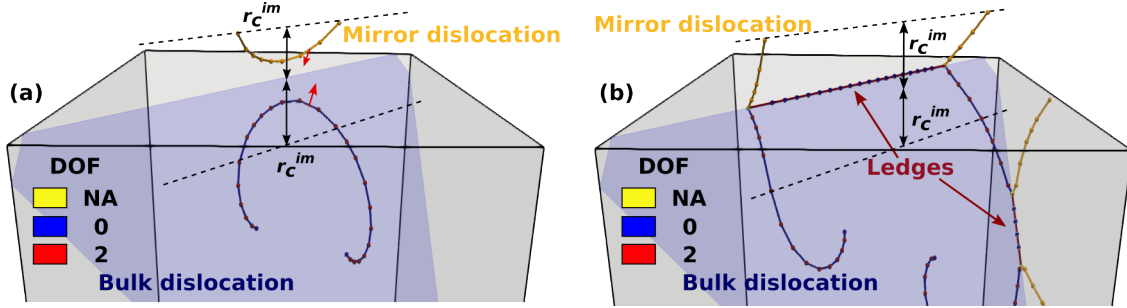


Figure 4: Dislocation interacting with surfaces in El-Numodis. (a) a dislocation close to a surface by a distance r_c^{im} is mirrored using planar symmetry, (b) bulk and mirror dislocations react at the surface creating a surface ledge. Dislocation and ledge nodes are colored according to their Degree Of Freedom number (DOF). NA=Not Accounted.

2.6. Dislocation nucleation

Dislocation nucleation was originally introduced within DDD simulations by Fivel *et al.* who used a criterion on the macroscopic stress to model the nucleation of prismatic loops during nanoindentation [82]. More recently, Roy *et al.* investigated homogeneous dislocation nucleation in nanoparticles nucleating octagonal loops with characteristic size (imposed by the user) in high-stress regions further testing their expansion by a strict calculation of the Peach-Koehler force between two consecutive DDD time steps [83]. This kind of approach was consecutively extended or adapted by several groups [57,63,83]. At the atomic scale, SDN has shown to be a stochastic process that depends on both the local shear stress and temperature [51,84]. This kind of mechanism can be rationalized using the TST that connects the phenomenon frequency of occurrence to the local thermomechanical conditions through an activation energy, as it has been done *e.g.*, by Zhu *et al.* for SDN in metal nano-objects [51]. Recently the approach of Zhu was extended to investigate the influence of the local atomic environment on the SDN process accounting for the sharpness of surface corners and edges [85,86]. To provide a more realistic description of what is commonly done at the mesoscale, our approach benefits of the recent theoretical progresses made on the dislocation nucleation process. Indeed, the code uses a combination of dislocation harmonic TST and Kinetic Monte-Carlo (KMC) to identify the favorable homogeneous or heterogeneous dislocation nucleation sites using meshed activation data and a probabilistic approach. As suggested by the harmonic TST, the dislocation nucleation rate at finite temperature and site i is described by,

$$\nu_i = \nu_{0,i} \exp\left(-\frac{\Delta G_i(\sigma_i, T)}{k_B T}\right) \quad (5)$$

where $\nu_{0,i}$ is the local attempt frequency, ΔG_i is the Gibbs free energy of the dislocation nucleation process at site i , σ_i is the local stress and $k_B T$ is the Boltzmann factor.

Thus, the probability for a dislocation to nucleate at site i during time δt in El-Numodis is computed as,

$$\delta N_i = \nu_i \cdot \delta t \quad (6)$$

with

$$\delta t = \frac{1}{\sum_{i=1}^N \nu_i} \quad (7)$$

with N the total number of nucleation sites.

The frequency n_{KMC} at which the KMC algorithm is called is defined by $n_{KMC} = \delta t_{DDD} / \delta t$ per DDD step, where δt_{DDD} is the DDD timestep. n_{KMC} is adapted *on-the-fly* during the simulation based on possible ν_i variations induced by local stress changes. Dislocation nucleation activation energy ΔG_i and other characteristic parameters (critical nucleation radius and slip systems) can be set as non-local inputs or using tabulated data on a 2D or 3D grid to account for the site-dependence of the nucleation process. Corresponding dislocations are then generated into the simulation box as circular glissile loop (homogeneous nucleation) or truncated half or quarter loops (heterogenous nucleation) depending on the nucleation site location. Finally, El-Numodis is able to interpolate multiple stress or strain-dependent ΔG_i databases to model the dislocation nucleation sensitivity to the mechanical history of the virtual sample.

While a comprehensive study of the SDN process in ceramic nanoparticles using atomistically-informed El-Numodis will be the main focus of a forthcoming study, a simplified application of the dislocation nucleation process is presented in Figure 5. In this example, we use a cubic-shaped copper single crystal of $500 \times 500 \times 500$ nm³ size under constant load. SDN in the $\frac{1}{2}\langle 110 \rangle \{111\}$ slip systems at three hypothetical nucleation sites is considered *i.e.*, two top corners c_1 and c_2 and the middle of a single lateral surface labelled s . As in the work of Zhu *et al.* [51], we use the approximation of an homogeneous surface disordering temperature $\Delta S_i = \Delta H_i / T_{m,i}$, where ΔS_i is the activation entropy at site i , ΔH_i is the 0 K nucleation activation enthalpy and $T_{m,i}$ is the local surface disordering temperature ($\nu_{0,i} = 3.14 \cdot 10^{11}$ /s and $T_{m,i} = 700$ K whatever i). Corner and mid-surface activation enthalpies are set to $\Delta H_{c_1} = \Delta H_{c_2} = 0.2$ eV and $\Delta H_s = 0.5$ eV respectively, assuming SDN to be more efficient from corners than from mid-surface. A high-enough constant load is considered ($\sigma_{zz} = 1$ GPa) to guarantee dislocation nucleation and glide. For a sake of simplicity, the per-site activation nucleation energy is temporarily increased after each nucleation event to mimic the effect of internal stress relaxation that prevents overly correlated nucleation events.

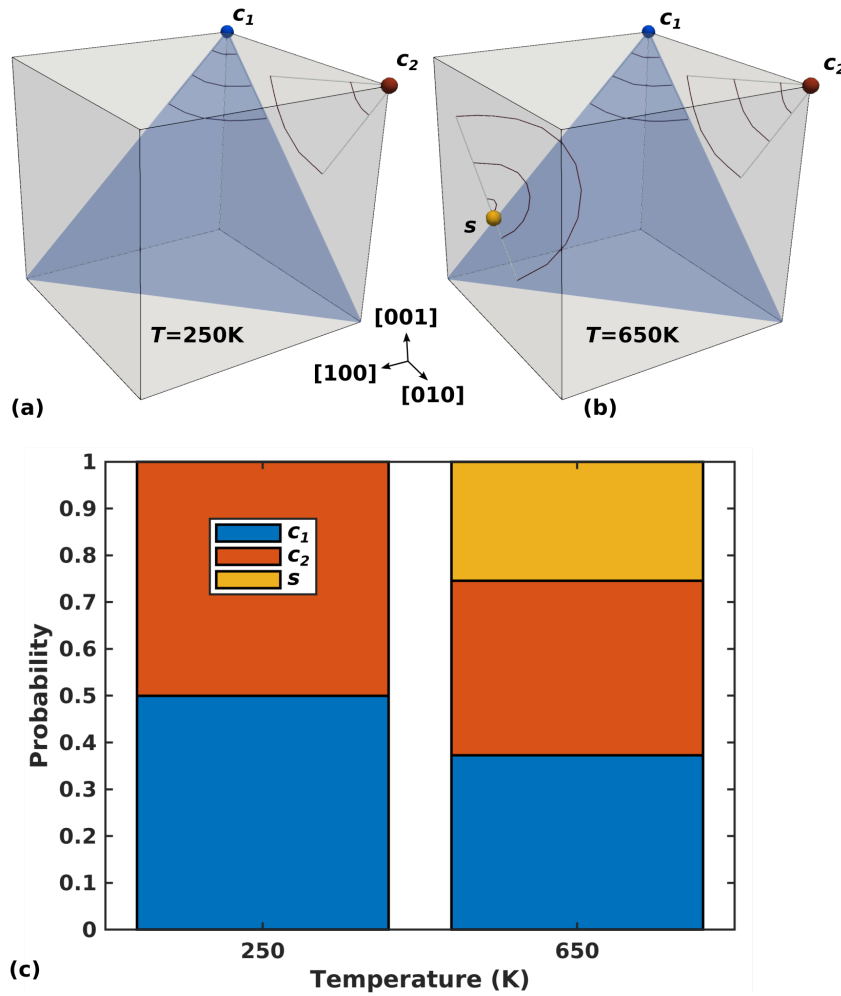


Figure 5: Dislocation nucleation at the surfaces of a cuboidal Cu sample under constant load ($\sigma_{zz}=1$ GPa) at (a) $T=250$ K and (b) $T=650$ K. (c) Nucleation probability $P_i = \nu_i / \sum_i \nu_i$ at corners c_1 and c_2 and mid-surface s computed at $T=250$ and 650 K.

Simulation performed at $T=250$ and 650 K are described Figure 5. El-Numodis promotes SDN originating only from c_1 and c_2 at $T=250$ K (Figure 5a) while nucleation events incoming from the three sites are observed at larger temperature (Figure 5b). This result is mainly explained by the site-dependence of the nucleation probability that is influenced by the temperature range as expected by the harmonic TST. Here, the probability to nucleate from a corner $P_c = \nu_c / \sum_i \nu_i \sim 0.5$ at $T=250$ K while its mid-surface counterpart is close to zero ($P_s = 6.47 \cdot 10^{-5}$) what justifies the lack of nucleation event from site s at low temperature. On the other hand, P_s increases up to ~ 0.25 when the temperature is increased up to 650 K as shown Figure 5c and nucleation from site s becomes more favorable.

2.7. Loading and feedback loops

El-Numodis handles displacement- and force-controlled BCs (Dirichlet and Neumann BCs, respectively) that can be set at each surface of the virtual sample allowing for constant strain rate or creep simulations. During constant strain rate simulation, a feedback control acting on stress is performed as described in Equation 8 using Neumann BCs. On the other hand, the sole SPM method is used during creep simulations.

$$\boldsymbol{\sigma}(\mathbf{S}, t) = \frac{1}{\boldsymbol{\Sigma}}(\dot{\boldsymbol{\epsilon}} \cdot t - \boldsymbol{\epsilon}^p(t)) \quad (8)$$

where $\boldsymbol{\sigma}(\mathbf{S}, t)$ is the applied stress tensor at the surface, t is the elapsed time, $\dot{\boldsymbol{\epsilon}}$ is the total strain rate tensor and $\boldsymbol{\epsilon}^p$ is the plastic strain tensor computed using the area swept by all moving dislocations. $\boldsymbol{\Sigma}$ is the corresponding compliance tensor.

3. Validation and applications

3.1. Dislocation stress field

El-Numodis benefits of both the singular and non-singular formulations for dislocation stress field (equations are provided as Supplementary Information). Figure 6 shows a comparison between El-Numodis DDD and the analytical formulation of the stress field using the Cai's non-singular theory [50]. From a technical point of view, a straight (edge or screw) dislocation is modeled assuming an infinite continuum using a simulation cell of size $1 \times 1 \times 1 \mu\text{m}^3$. The dislocation line is oriented along $z=[001]$ and the stress field is illustrated in the (x,y) plan at $z=0.5 \mu\text{m}$. Copper lattice parameter ($a_0=3.61 \text{ \AA}$) and isotropic elasticity ($\lambda=77.3 \text{ GPa}$, $\mu=42.0 \text{ GPa}$, $\nu=0.324$) are used for the example. Overall, results show a good agreement between analytical and El-Numodis solutions. One could notice that changing the BCs from periodic to fixed-BCs as well as short variations of cell dimensions along x and y do not significantly impact the results for the investigated size range.

3.2. Edge dislocation and free surface

Here we test El-Numodis reliability in the context of the stress-free BC problem by investigating how the stress field of an edge dislocation is modified in the vicinity of a free surface, as described in Figure 7a. In their seminal work, Hirth and Lothe proposed an analytical solution to this problem that relies on the concept of image dislocation [26]. Indeed, the authors demonstrate that most of the stress components induced by an infinite edge dislocation can be cancelled at a surface by adding a so-called image dislocation located on the other side of the surface. The image dislocation is characterized by i) the same line direction and infinite length, ii) an opposite Burgers vectors $-\mathbf{b}$ and iii) the same dislocation-to-surface distance l than the original

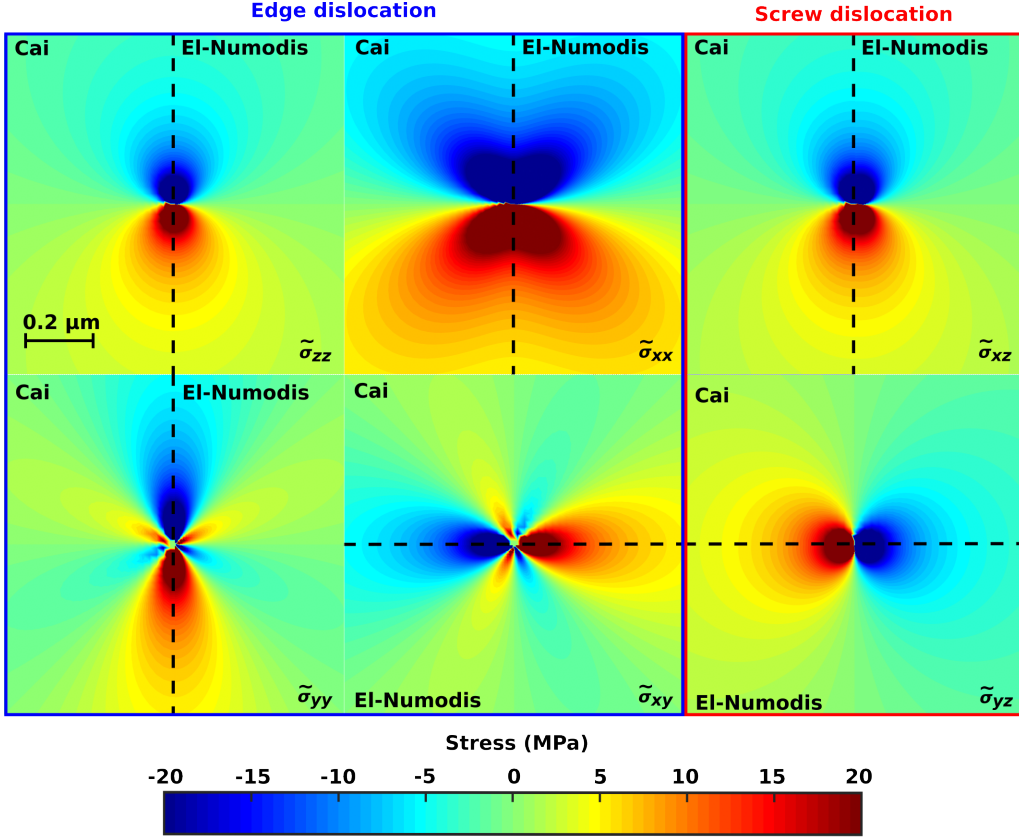


Figure 6: Comparison between El-Numodis and analytical formulations of edge and screw dislocation stress fields in the framework of the non-singular theory of Cai [50].

dislocation. In addition, they use an Airy stress $\hat{\sigma}^{Airy}$ superimposed to the self $\tilde{\sigma}$ and image dislocation $\hat{\sigma}^{im}$ stress-fields to ensure the complete vanishing of all the stress components at the free surface (*i.e.*, for $x=l$), without modifying the long-range stress distribution within the sample,

$$\tilde{\sigma}_{ij} + \hat{\sigma}_{ij}^{im} + \hat{\sigma}_{ij}^{Airy} = 0, \text{ for } x = l \quad (9)$$

with $\hat{\sigma}_{ij}^{im}$ the stress components of the image dislocation.

Within the Hirth and Lothe 2D formulation, the Airy stress components that verify the stress-free conditions of the x -oriented surface are given by,

$$\sigma_{xx}^{Airy} = -\frac{2\mu b l x y}{\pi(1-\nu)r^6} [3(l-x)^2 - y^2] \quad (10)$$

$$\sigma_{xy}^{Airy} = -\frac{\mu b l}{\pi(1-\nu)r^6} [(l-x)^4 + 2x(l-x)^3 + 6xy^2(l-x) - y^4] \quad (11)$$

where $r = (l^2 + y^2)^{1/2}$

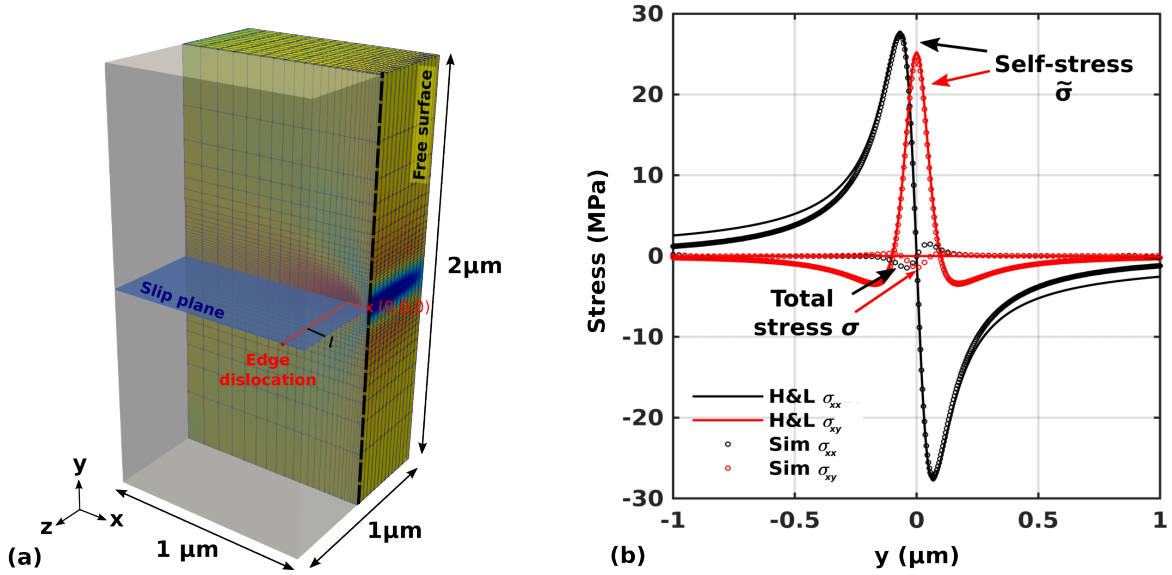


Figure 7: Edge dislocation and free surface: stress-field prediction comparison between El-Numodis simulation (Sim) and Hirth and Lothe (H&L) theoretical model. (a) Simulation setup, (b) Dislocation self-stress $\tilde{\sigma}$ and total stress σ variations along y for a $30 \times 60 \times 30$ elements mesh with special refine in the vicinity of the dislocation (Gmsh Bump=-4.9 and Progression=1.3). Data are plotted along a virtual line crossing the free surface.

The Hirth and Lothe model presented in Equation 9 relies on a stress summation very close the one used in the SPM. Thus, one way to test El-Numodis implementation is to verify that the FEM stress correction computed by the code correctly reproduces the Hirth and Lothe theoretical predictions of Airy and image stresses *i.e.*, $\hat{\sigma} = \hat{\sigma}^{im} + \hat{\sigma}^{Airy}$. To test this hypothesis, we design $1 \times 2 \times 1 \mu\text{m}^3$ simulation cells including a finite-length edge dislocation (line along z , Burgers vector along x) located at a distances $l = 0.1 \mu\text{m}$ from a surface located at $x = 0$. Simulation volumes are meshed using 8-nodes hexahedron elements. Various geometries are tested including elements distributions from $30 \times 30 \times 30$ up to $120 \times 120 \times 120$. Figure 7a shows a $30 \times 60 \times 30$ volume with mesh refinement near the dislocation performed using Gmsh (Bump=-4.9 and Progression=1.3) [87]. As in the previous test-case, copper lattice and elastic properties are used. In the simulation, traction-free BC is applied to the x free-surface while zero fixed displacement is used on the opposite side (other surfaces are not considered). The total stress σ and the dislocation self-stress $\tilde{\sigma}$ obtained are presented in Figure 7b as plotted along a vertical line passing along the free-surface. Results confirm El-Numodis ability to reproduce theoretical $\tilde{\sigma}$, as already shown in Figure 6. In addition, the plot of σ allows for a direct comparison between the FEM correction $\hat{\sigma}$ and the Hirth and Lothe model $\hat{\sigma}^{im} + \hat{\sigma}^{Airy}$. The total stress components σ_{xx} and σ_{xy} show a significant decrease at the surface (originally equal to the self-stress) what confirms the correct implementation of

the superposition algorithm within El-Numodis. This result applies almost everywhere except close to $y=0$, where spurious stresses are observed. These discrepancies are attributed to the mesh refinement in this region (where large stress gradients are shown) as well as to the intrinsic difference between the 2D Hirth and Lothe model and the 3D finite-size simulation. One can notice that similar stress singularities at free-surface were already observed in simulations using the SPM [27] or the DCM approach [42, 88].

Still for this test-case, Figure 8 illustrates the influence of the mirror dislocation method on El-Numodis stress field correction. Results show a qualitative agreement between simulated $\hat{\boldsymbol{\sigma}}$ (or $\hat{\boldsymbol{\sigma}}-\hat{\boldsymbol{\sigma}}^{im}$, depending if the mirror image method is turned off or on) and the $\hat{\boldsymbol{\sigma}}^{Airy}$ of the Hirth and Lothe model. Overall, using the mirror image method with FEM to compute the image stress improves the results allowing for less refined meshes. However, such an improvement has limitations as emphasized by the $y = 0$ region where data for 60 and 120 elements simulations saturate. Thus, the residual stress in the $y = 0$ region also observed Figure 7b is neither significantly sensitive to simulation cell size variations or nor to the mesh refinement.

3.3. Square dislocation loop and free surface

In this section, we use El-Numodis to solve the stress-free BC problem in the case of a dislocation square loop located in the vicinity of a free surface. Curved dislocation stress field can be computed using linear elasticity and surface integration built out of the dislocation curvature [75, 89, 90],

$$\sigma_{pq}(\mathbf{x}') = - \int b_s C_{srkl} C_{pqmj} \frac{\partial}{\partial x'_j} G_{mk,j}(\mathbf{x}, \mathbf{x}') dS_r \quad (12)$$

where \mathbf{C} is the elastic stiffness and \mathbf{G} is the Green tensor associated to a particular material.

In an infinite medium, Equation 12 can be reduced into a simple integral computed along the dislocation line using the Stokes theorem. Gosling and Willis expanded this approach to a finite-size domain using Equation 13 where \mathbf{S}^∞ and $\hat{\mathbf{S}}$ are kernels associated to infinite and finite-size media respectively [90]. The integral of $\hat{\mathbf{S}}$ directly leads to the image stress $\hat{\boldsymbol{\sigma}}$; It will be referred as the Gosling-Willis solution in the following (more details on this approach can be found *e.g.*, in Ref. [75]).

$$\sigma_{pq}(\mathbf{x}') = - \oint_C b_s [S_{pqrs}^\infty(\mathbf{x} - \mathbf{x}') + \hat{S}_{pqrs}(\mathbf{x}, \mathbf{x}')] dx \quad (13)$$

The El-Numodis simulation setup used to model the square loop and surface interactions is presented Figure 9a. A copper $\langle 100 \rangle$ -oriented simulation cell with dimensions

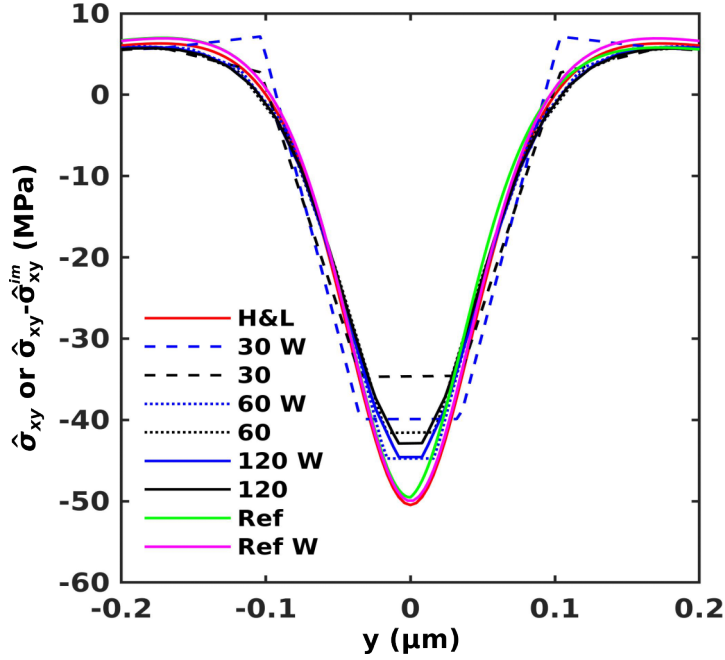


Figure 8: El-Numodis $\hat{\sigma}_{xy}$ (or $\hat{\sigma}_{xy} - \hat{\sigma}_{xy}^{im}$ when accounting the mirroring dislocation method) correction as function of mesh refinement. Simulations are performed for mesh discretization of 30 (dashed curves), 60 (dotted curves) and 120 (full curves) 8-nodes hexahedron elements in the three directions of space, using the Weygand's mirror dislocation method (W) or not. *Ref* curves rely on the aforementioned $30 \times 60 \times 30$ with particular mesh refinement near the dislocation using Gmsh (Bump=-4.9 and Progression=1.3). Results are compared to the $\hat{\sigma}_{xy}^{Airy}$ of the Hirth & Lothe model (H&L, red curve). Data are plotted along a vertical line passing by the middle of the x -surface as shown in Figure 7a.

of $5 \times 5 \times 2.5 \mu\text{m}^3$ is meshed with 8-nodes hexahedron elements further refined near the $[001]$ bottom free surface. A $\frac{1}{2}[\bar{1}01](111)$ square dislocation loop axis-aligned with z and with edge lengths of about $0.5 \mu\text{m}$ is introduced at $0.37 \mu\text{m}$ of the bottom- z surface at which stress-free BCs are applied. As in the previous case, zero displacement fixed BCs are used for the opposite z surface while remaining surfaces are not considered as boundaries in the simulation. The mirroring dislocation method is off here.

Results are presented in Figure 9b and 10. On one hand, Figure 9b shows the variations of the FEM stress correction $\hat{\sigma}$ as plotted along the z -axis starting from the free surface up to $2 \mu\text{m}$ and passing through the center of the dislocation loop. Here the results illustrate that El-Numodis is particularly suited to reproduce the Gosling-Willis theoretical solution. On the other hand, $\tilde{\sigma}$, $\hat{\sigma}$ and $\tilde{\sigma} + \hat{\sigma}$ stress maps plotted at the bottom- z surface are shown in Figure 10. El-Numodis allows for the decrease of the various stress components by more than a factor 5 with only few MPa leftover at the surface. This test further confirms the ability of El-Numodis to solve stress-free BVPs.

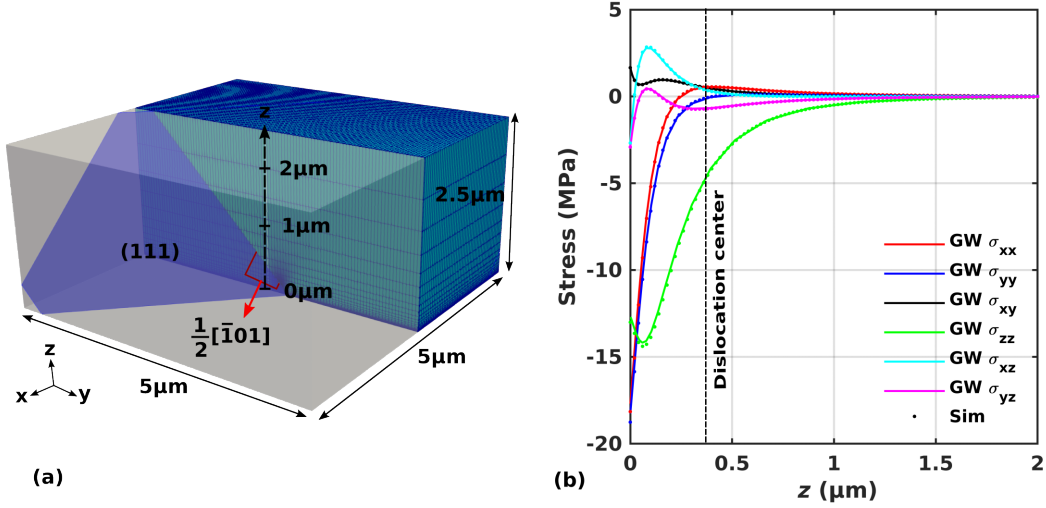


Figure 9: Dislocation square loop in the vicinity of a free surface: image stress field comparison between El-Numodis simulation (Sim) and the Gosling-Willis (GW) theoretical model (a) Simulation setup, (b) Image stress components $\hat{\sigma}_{ij}$ as measured along a vertical line passing by the middle of the dislocation square loop. El-Numodis results (dots) are compared to the Gosling-Willis model (curves).

3.4. Example of application: thin film tensile test

For this final application, El-Numodis is confronted to classical DDD (*i.e.*, standalone Numodis) performing tensile tests on a model thin film. A $\langle 100 \rangle$ -oriented Cu thin film of 250 nm thickness is generated and meshed using eight nodes hexahedrons discretized with 20 points along $[010]$ and $[001]$ directions while 10 points are used along $[100]$. The initial dislocation microstructure is identical in both simulations. It is made of 25 Frank-Read sources of 0.2 μm length randomly distributed on the various slip systems of the FCC crystal structure. The defects distribution is biased using a cutoff to avoid overlapping and boundary crossing. Constant strain-rate simulation ($\dot{\epsilon}=10^{-6}$ /ns) is performed pulling from one of the (001) lateral surface while the opposite one is kept fixed. Other surfaces are set stress-free in El-Numodis. The mirror-image dislocation method is used in El-Numodis simulation only with a cutoff distance of 60 nm while free-BCs are used in the pure DDD simulation. Equation 8 feedback loop is used to correct the applied stress at the boundary in both simulations.

Computed stress-strain curves are shown in Figure 11a. Both SPM and DDD simulations are characterized by an initial elastic load up to the activation of the first Frank-Read sources. The pure DDD exhibits a higher yield stress when compared to El-Numodis (196 and 175 MPa, respectively) and, overall, a harder mechanical response

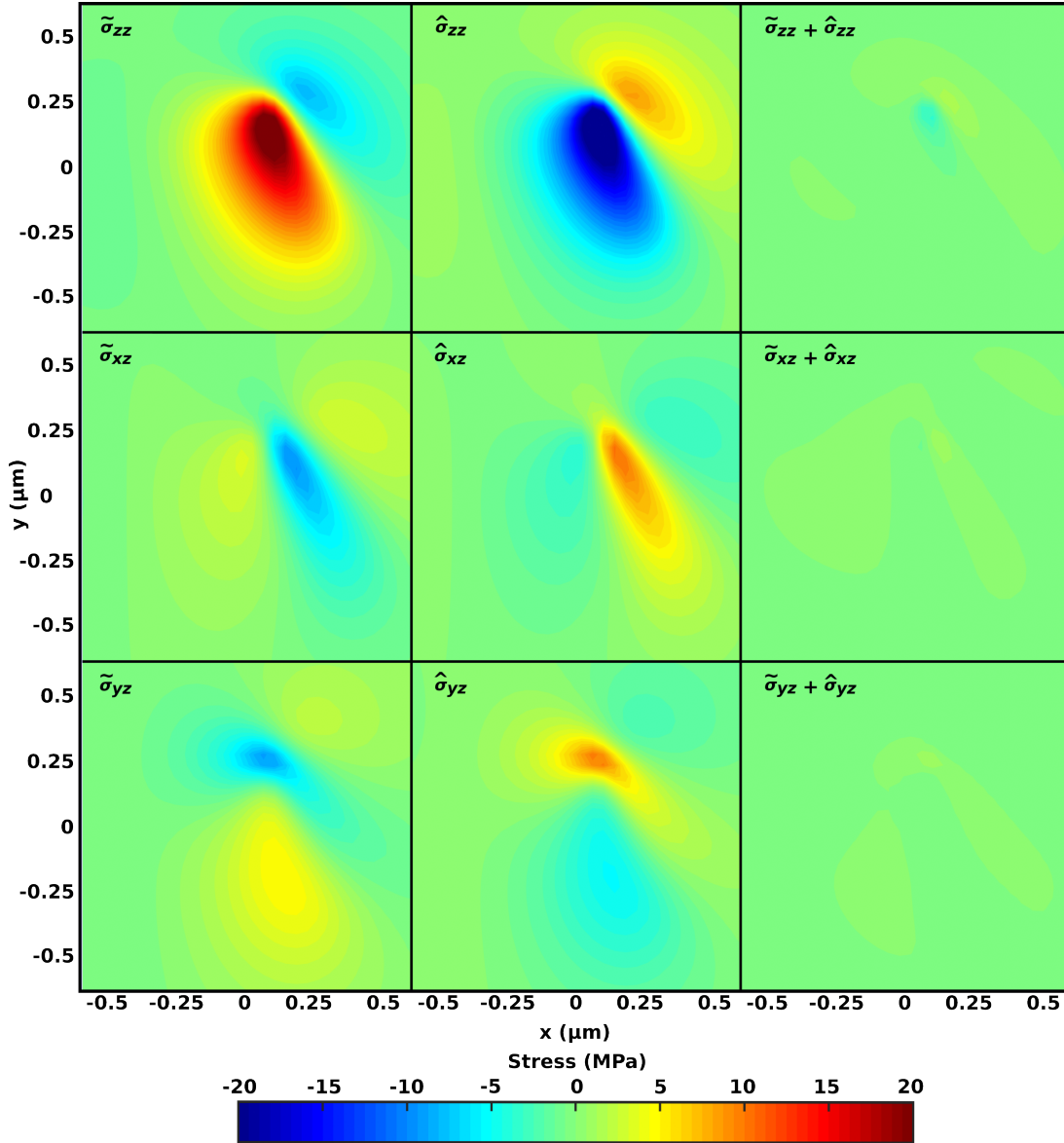


Figure 10: Stress components of $\tilde{\sigma}$, $\hat{\sigma}$ and total stress $\tilde{\sigma} + \hat{\sigma}$ computed using El-Numodis at the bottom- z surface close to a dislocation square loop.

all along the simulation. Figure 11b shows both dislocation microstructures in the early stage of deformation. One can easily identify the prior activation of parts of the Frank-Read sources close to the surfaces in the SPM simulation, as indicated by the red arrows in Figure 11b. On the other hand, the DDD simulation does not show any influence of the surfaces and the applied stress within the sample is homogeneous what promotes the activation of Frank-Read sources localized in high-Schmid factor slip systems only. Here surfaces in the El-Numodis simulation behave as sinks that help the opening of the Frank-Read sources towards the surfaces in a similar way that in the aforementioned TEM lamella case [46]. Moreover, accounting for surfaces significantly influences the

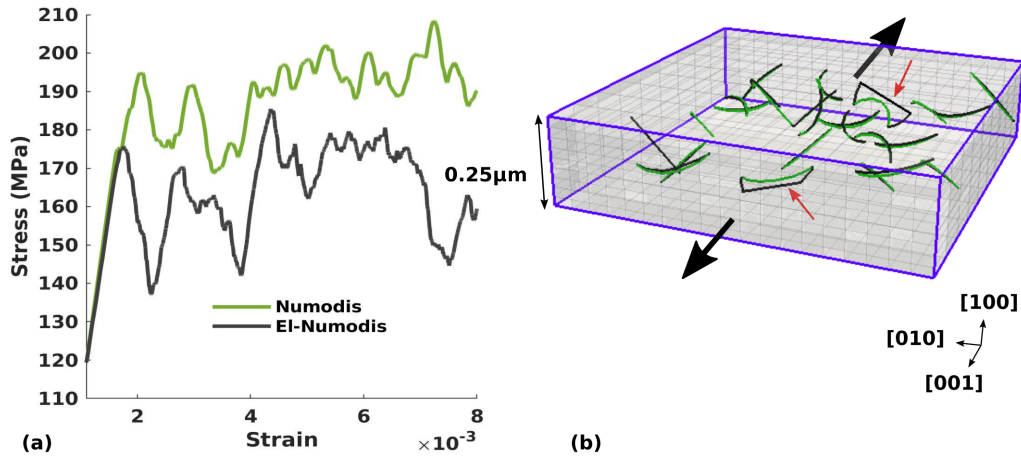


Figure 11: Thin film tensile test: standalone Numodis (DDD) *vs.* El-Numodis (SPM). (a) stress-strain curves, (b) Comparative dislocation microstructures at the yield point (black=Numodis, green=El-Numodis). Red arrows highlight early emerging dislocations in the El-Numodis simulation. Black arrows refer to the tensile direction.

dislocation dynamics and elementary reaction processes between dislocations. For example, some junction reactions initially observed in the pure DDD simulation have shown to be anticipated by the surface-induced pump-out process modeled using El-Numodis and the SPM method. This process influences the whole plastic regime which is shown to be softer when accounting for the physics of surfaces. Additional simulations show that increasing the film thickness tends to reduce the gap between pure DDD and the SPM mechanical responses while increasing the cutoff used in the mirroring dislocation method tends to decrease the yield stress.

4. Conclusion

Here we present a tool based on the SPM method called El-Numodis to model dislocation dynamics in finite-size environments. The approach couples the nodal DDD code Numodis and the Elmer FEM code used here as an elastic solver of BVPs where the BCs are corrected by the effect originating from the presence of dislocations. El-Numodis refers on three external drivers that ensure the various operations and exchange between the DDD and FEM parent codes. It benefits of specific modern developments including the non-singular dislocation theory of Cai [50], the mirror image method [27] as well as a Monte-Carlo based dislocation nucleation algorithm that allow for more physics-based dislocation simulations at the micro- and nano-scales. From a technical viewpoint, these developments make El-Numodis particularly versatile (and not more complex) than its original DDD parent code Numodis [47, 48]. In this study, El-Numodis was widely benchmarked including several test-cases designed to investigate interactions between

dislocation and surfaces. Among others, straight and square-shaped dislocations were tested in the vicinity of free-surfaces where El-Numodis has shown to be particularly suited to relax surface stress fields. A dislocation nucleation algorithm using a Monte-Carlo approach and the TST was also introduced. It will be soon extended to the study of dislocation nucleation in nanoparticles using energy barrier databases [85]. Finally, last tensile tests applications performed on model thin films completes the picture of El-Numodis potential. Besides ongoing improvements as on force calculation [91,92] or Gauss integration [93], we believe that El-Numodis is now ready for various kinds of applications in the field of small-scale mechanics.

Acknowledgements

This work was funded by INSA-Lyon and the Agence National de Recherche, grant no. ANR-20-CE09-0015 (ANR SASHA).

Data availability statement

All data that support the findings of this study are included within the article (and any supplementary files). El-Numodis is available on-demand at laurent.dupuy@cea.fr and jonathan.amodeo@cncrs.fr.

Bibliography

- [1] B Devincere and L P Kubin. Mesoscopic simulations of dislocations and plasticity. Materials Science and Engineering A, 234:8 – 14, 1997.
- [2] M. Fivel, M. Verdier, and G. Canova. 3D simulation of a nanoindentation test at a mesoscopic scale. Materials Science and Engineering A, 234-236:923–926, 1997.
- [3] VV Bulatov, LL Hsiung, M Tang, A Arsenlis, MC Bartelt, W Cai, JN Florando, M Hiratani, M Rhee, and G Hommes. Dislocation multi-junctions and strain hardening. Nature, 440(7088):1174 – 1178, 2006.
- [4] Yu U Wang, YM Jin, AM Cuitino, and AG Khachaturyan. Nanoscale phase field microelasticity theory of dislocations: model and 3d simulations. Acta materialia, 49(10):1847–1857, 2001.
- [5] D Rodney, Y Le Bouar, and A Finel. Phase field methods and dislocations. Acta materialia, 51(1):17–30, 2003.
- [6] Michael P Allen et al. Introduction to molecular dynamics simulation. Computational soft matter: from synthetic polymers to proteins, 23(1):1–28, 2004.
- [7] Luis A Zepeda-Ruiz, Alexander Stukowski, Tomas Ooppelstrup, and Vasily V Bulatov. Probing the limits of metal plasticity with molecular dynamics simulations. Nature, 550(7677):492–495, 2017.
- [8] Tamas Varady, Ralph R Martin, and Jordan Cox. Reverse engineering of geometric models—an introduction. Computer-aided design, 29(4):255–268, 1997.
- [9] ZL Liu, Z Zhuang, XM Liu, XC Zhao, and ZH Zhang. A dislocation dynamics based higher-order crystal plasticity model and applications on confined thin-film plasticity. International Journal of Plasticity, 27(2):201–216, 2011.
- [10] Ghiath Monnet, Ludovic Vincent, and Benoit Devincere. Dislocation-dynamics based crystal plasticity law for the low-and high-temperature deformation regimes of bcc crystal. Acta

- Materialia, 61(16):6178–6190, 2013.
- [11] David Cereceda, Martin Diehl, Franz Roters, Dierk Raabe, J Manuel Perlado, and Jaime Marian. Unraveling the temperature dependence of the yield strength in single-crystal tungsten using atomistically-informed crystal plasticity calculations. International Journal of Plasticity, 78:242–265, 2016.
 - [12] Luc Portelette, Jonathan Amodeo, Bruno Michel, and Ronan Madec. Athermal dislocation strengthening in uo_2 . Journal of Nuclear Materials, 538:152157, 2020.
 - [13] An Hui Lu, E. L. Salabas, and Ferdi Schüth. Magnetic nanoparticles: Synthesis, protection, functionalization, and application. Angewandte Chemie - International Edition, 46(8):1222–1244, 2007.
 - [14] Hong-wang Zhang, Yi Liu, and Shou-heng Sun. Synthesis and assembly of magnetic nanoparticles for information and energy storage applications. Frontiers of Physics in China, 5(4):347–356, 2010.
 - [15] Mustafa Akbulut. Nanoparticle-Based Lubrication Systems. Journal of Powder Metallurgy and Mining, 01(01):1–3, 2012.
 - [16] Wei Dai, Bassem Kheireddin, Hong Gao, and Hong Liang. Roles of nanoparticles in oil lubrication. Tribology International, 102:88–98, 2016.
 - [17] Xuezhou Li, Chenyu Wang, Jianlin Xiao, and Yanguo Qin. Applications of nanotechnology in hip implants. Advanced Materials Research, 662:218–222, 2013.
 - [18] Masaki Taneike, Fujio Abe, and Kota Sawada. Creep-strengthening of steel at high temperatures using nano-sized carbonitride dispersions. Nature, 424(6946):294–296, 2003.
 - [19] Riccardo Casati and Maurizio Vedani. Metal matrix composites reinforced by nano-particles—a review. Metals, 4(1):65–83, 2014.
 - [20] Julia Greer and Jeff De Hosson. Plasticity in small-sized metallic systems: intrinsic versus extrinsic size effect. Progress in Materials Science, 56(6):654 – 724, 2011.
 - [21] Dan Mordehai, Omer David, and Roman Kositski. Nucleation-controlled plasticity of metallic nanowires and nanoparticles. Advanced Materials, 305:1706710 – 17, 07 2018.
 - [22] Andrew T Jennings and Julia R Greer. Heterogeneous dislocation nucleation from surfaces and interfaces as governing plasticity mechanism in nanoscale metals. Journal of Materials Research, 26(22):2803 – 2814, 11 2011.
 - [23] C R Weinberger, Andrew T Jennings, Keonwook Kang, and Julia R Greer. Atomistic simulations and continuum modeling of dislocation nucleation and strength in gold nanowires. Journal of the Mechanics and Physics of Solids, 60(1):84 – 103, 01 2012.
 - [24] Jonathan Amodeo and Khalid Lizoul. Mechanical properties and dislocation nucleation in nanocrystals with blunt edges. Materials and Design, 135:223 – 231, 2017.
 - [25] Inas Issa, Lucile Joly-Pottuz, Jonathan Amodeo, David J. Dunstan, Claude Esnouf, Julien Réthoré, Vincent Garnier, Jérôme Chevalier, and Karine Masenelli-Varlot. From dislocation nucleation to dislocation multiplication in ceramic nanoparticle. Materials Research Letters, 9(6):278–283, 2021.
 - [26] J P Hirth and J Lothe. Theory of dislocations. New York: John Willey and Sons, 01 1982.
 - [27] D. Weygand, L. H. Friedman, E. Van Der Giessen, and A. Needleman. Aspects of boundary-value problem solutions with three-dimensional dislocation dynamics. Modelling and Simulation in Materials Science and Engineering, 10(4):437–468, 2002.
 - [28] A M Minor, J W Morris, and E A Stach. Quantitative in situ nanoindentation in an electron microscope. Applied Physics Letters, 79(11):1625, 2001.
 - [29] Fredrik Östlund, Karolina Rzepiejewska-Malyska, Klaus Leifer, Lucas M Hale, Yuye Tang, R Ballarini, William W Gerberich, and Johann Michler. Brittle-to-ductile transition in uniaxial compression of silicon pillars at room temperature. Advanced Functional Materials, 19(15):2439 – 2444, 08 2009.
 - [30] M Legros, D S Gianola, and C Motz. Quantitative In Situ Mechanical Testing in Electron Microscopes. MRS bulletin, 35(5):354 – 360, 2010.

- [31] David B. Williams and C. Barry Carter. The Transmission Electron Microscope, pages 3–17. Springer US, Boston, MA, 1996.
- [32] S. Zaefferer. A critical review of orientation microscopy in SEM and TEM. Crystal Research and Technology, 46(6):607–628, 2011.
- [33] William Gerberich, Ellad B Tadmor, Jeffrey Kysar, Jonathan A Zimmerman, Andrew M Minor, Izabela Szlufarska, Jonathan Amodeo, Benoit Devincere, Eric Hintsala, and R Ballarini. Review Article: Case studies in future trends of computational and experimental nanomechanics. Journal of Vacuum Science & Technology A: Vacuum, Surfaces, and Films, 35(6):060801 – 20, 2017.
- [34] Jonathan Amodeo and Laurent Pizzagalli. Modeling the mechanical properties of nanoparticles: a review. Comptes Rendus. Physique, 22(S3):1–32, 2021.
- [35] B Devincere and L P Kubin. The modelling of dislocation dynamics: elastic behaviour versus core properties. Philosophical Transactions: Mathematical, 355(1731):2003 – 2012, 1997.
- [36] B Devincere, R Madec, G Monnet, S Queyreau, R Gatti, and L Kubin. Modeling crystal plasticity with dislocation dynamics simulations: the ‘microMegas’ code. Mechanics of nano-objects, pages 81 – 100. Paris, Presses des Mines, 10 2011.
- [37] A Arsenlis, W Cai, M Tang, M Rhee, T Ooppelstrup, G Hommes, T G Pierce, and V V Bulatov. Enabling strain hardening simulations with dislocation dynamics. Modelling and Simulation in Materials Science and Engineering, 15(6):553, 2007.
- [38] Marc C. Fivel. Discrete dislocation dynamics: an important recent break-through in the modelling of dislocation collective behaviour. Comptes Rendus Physique, 9(3-4):427–436, 2008.
- [39] Erik Van der Giessen and Alan Needleman. Discrete dislocation plasticity: A simple planar model. Modelling and Simulation in Materials Science and Engineering, 3(5):689–735, 1995.
- [40] C Lemarchand, J L Chaboche, B Devincere, and L P Kubin. Multiscale modelling of plastic deformation. Le Journal de Physique IV, 09(PR9):Pr9–271 – Pr9–277, 09 1999.
- [41] A Vattré, B Devincere, F Feyel, R Gatti, S Groh, O Jamond, and A Roos. Modelling crystal plasticity by 3D dislocation dynamics and the finite element method: The Discrete-Continuous Model revisited. Journal of the Mechanics and Physics of Solids, 63(1):491–505, 2014.
- [42] O Jamond, R Gatti, A Roos, and B Devincere. Consistent formulation for the Discrete-Continuous Model: Improving complex dislocation dynamics simulations. International Journal of Plasticity, 80(C):19 – 37, 05 2016.
- [43] T Mura. Micromechanics of Defects in Solids. Martinus Nijhoff publishers, Dordrecht, 11 1987.
- [44] N Bertin, M V Upadhyay, C Pradalier, and L Capolungo. A FFT-based formulation for efficient mechanical fields computation in isotropic and anisotropic periodic discrete dislocation dynamics. Modelling and Simulation in Materials Science and Engineering, 23(6):065009, 2015.
- [45] Siwen Gao, Marc Fivel, Anxin Ma, and Alexander Hartmaier. Influence of misfit stresses on dislocation glide in single crystal superalloys: A three-dimensional discrete dislocation dynamics study. Journal of the Mechanics and Physics of Solids, 76:276–290, 2015.
- [46] Aaron A Kohnert, Hareesh Tummala, Ricardo A Lebensohn, Carlos N Tomé, and Laurent Capolungo. On the use of transmission electron microscopy to quantify dislocation densities in bulk metals. Scripta Materialia, 178:161–165, 2020.
- [47] Julie Drouet, Laurent Dupuy, Fabien Onimus, Frédéric Momprou, Simon Perusin, and A Ambard. Dislocation dynamics simulations of interactions between gliding dislocations and radiation induced prismatic loops in zirconium. Journal of Nuclear Materials, 449(1-3):252 – 262, 06 2014.
- [48] X.J. Shi, L. Dupuy, B. Devincere, D. Terentyev, and L. Vincent. Interaction of $< 100 >$ dislocation loops with dislocations studied by dislocation dynamics in α -iron. Journal of Nuclear Materials, 460:37–43, 2015.
- [49] M Malinen and Peter Råback. Elmer finite element solver for multiphysics and multiscale problems. Multiscale Model. Methods Appl. Mater. Sci., 19:101 – 113, 01 2013.
- [50] W Cai, A Arsenlis, C Weinberger, and V Bulatov. A non-singular continuum theory of dislocations.

- Journal of the Mechanics and Physics of Solids*, (54):561–587, 2006.
- [51] T Zhu, J Li, Amit Samanta, Austin Leach, and Ken Gall. Temperature and strain-rate dependence of surface dislocation nucleation. *Physical Review Letters*, 100(2):025502, 2008.
 - [52] J Lepinoux and L P Kubin. The dynamic organization of dislocation structures: a simulation. *Scripta Metallurgica*, 21(6):833 – 838, 1987.
 - [53] R Madec, B Devincere, and L P Kubin. From dislocation junctions to forest hardening. *Physical Review Letters*, 89(25):2555081 – 2555084, 2002.
 - [54] Tomas Diaz De la Rubia, Hussein M Zbib, Tariq A Khraishi, Brian D Wirth, Max Victoria, and Maria Jose Caturla. Multiscale modelling of plastic flow localization in irradiated materials. *Nature*, 406(6798):871–874, 2000.
 - [55] Athanasios Arsenlis, Moono Rhee, Gregg Hommes, Robert Cook, and Jaime Marian. A dislocation dynamics study of the transition from homogeneous to heterogeneous deformation in irradiated body-centered cubic iron. *Acta Materialia*, 60(9):3748–3757, 2012.
 - [56] C Déprés, C F Robertson, and M C Fivel. Low-strain fatigue in AISI 316L steel surface grains: a three-dimensional discrete dislocation dynamics modelling of the early cycles I. Dislocation microstructures and mechanical behaviour. *Philosophical Magazine A*, 84(22):2257 – 2275, 2004.
 - [57] J Gagel, D Weygand, and P Gumbsch. Formation of extended prismatic dislocation structures under indentation. *Acta Materialia*, 111(C):399 – 406, 06 2016.
 - [58] Hyung Jun Chang, Heung Nam Han, and Marc Fivel. Multiscale modelling of nanoindentation. In *Key Engineering Materials*, volume 345, pages 925–930, 2007.
 - [59] Jonathan Amodeo, P Carrez, B Devincere, and P Cordier. Multiscale modelling of MgO plasticity. *Acta Materialia*, 59(6):2291 – 2301, 2011.
 - [60] Jonathan Amodeo, B Devincere, Ph Carrez, and P Cordier. Dislocation reactions, plastic anisotropy and forest strengthening in MgO at high temperature. *Mechanics of Materials*, 71:62 – 73, 2014.
 - [61] R Reali, J M Jackson, J Van Orman, D J Bower, P Carrez, and P Cordier. Modeling viscosity of (Mg,Fe)O at lowermost mantle conditions. *Physics of the Earth and Planetary Interiors*, 287:65 – 75, 01 2019.
 - [62] L P Kubin. *Dislocations, Mesoscale Simulations and Plastic Flow*. Oxford University Press. Oxford University Press, 04 2013.
 - [63] Giacomo Po, Mamdouh S Mohamed, Tamer Crosby, Can Erel, Anter El-Azab, and Nasr Ghoniem. Recent Progress in Discrete Dislocation Dynamics and Its Applications to Micro Plasticity. *JOM*, 66(10):2108 – 2120, 09 2014.
 - [64] Yang Li, Max Boleininger, Christian Robertson, Laurent Dupuy, and Sergei L. Dudarev. Diffusion and interaction of prismatic dislocation loops simulated by stochastic discrete dislocation dynamics. *Physical Review Materials*, 3(7):073805, 2019.
 - [65] Wei Cai, Athanasios Arsenlis, Christopher R. Weinberger, and Vasily V. Bulatov. A non-singular continuum theory of dislocations. *Journal of the Mechanics and Physics of Solids*, 54(3):561–587, 2006.
 - [66] Pierre-Antoine Geslin and David Rodney. Thermal fluctuations of dislocations reveal the interplay between their core energy and long-range elasticity. *Physical Review B*, 98(17):174115, 2018.
 - [67] Yi Hu, BA Szajewski, D Rodney, and WA Curtin. Atomistic dislocation core energies and calibration of non-singular discrete dislocation dynamics. *Modelling and Simulation in Materials Science and Engineering*, 28(1):015005, 2019.
 - [68] N. Bertin, W. Cai, S. Aubry, and V. V. Bulatov. Core energies of dislocations in bcc metals. *Physical Review Materials*, 5:025002, 2021.
 - [69] Vasily Bulatov and W Cai. *Computer Simulations of Dislocations*. Oxford University Press. Oxford University Press, 11 2006.
 - [70] V Savolainen, J Heikonen, J Ruokolainen, O Anttila, M Laakso, and J Paloheimo. Simulation of large-scale silicon melt flow in magnetic czochralski growth. *Journal of crystal growth*, 243(2):243–260, 2002.
 - [71] Esko Järvinen, Peter Råback, Mikko Lyly, and Juha-Pekka Salenius. A method for partitioned

- fluid–structure interaction computation of flow in arteries. Medical engineering & physics, 30(7):917–923, 2008.
- [72] O Gagliardini, T Zwinger, F Gillet-Chaulet, G Durand, L Favier, B de Fleurian, R Greve, M Malinen, C Martín, P Råback, et al. Capabilities and performance of elmer/ice, a new-generation ice sheet model. Geoscientific Model Development, 6(4):1299–1318, 2013.
- [73] Janne Keränen, Jenni Pippuri, Mika Malinen, Juha Ruokolainen, Peter Råback, Mikko Lyly, and Kari Tammi. Efficient parallel 3-d computation of electrical machines with elmer. IEEE Transactions on Magnetics, 51(3):1–4, 2015.
- [74] Juris Vencels, Peter Råback, and Vadims Geža. Eof-library: Open-source elmer fem and openfoam coupler for electromagnetics and fluid dynamics. SoftwareX, 9:68–72, 2019.
- [75] M. C. Fivel, T. J. Gosling, and G. R. Canova. Implementing image stresses in a 3D dislocation simulation. Modelling and Simulation in Materials Science and Engineering, 4(6):581–596, 1996.
- [76] Robert D Falgout and Ulrike Meier Yang. hypre: A library of high performance preconditioners. In Computational Science-ICCS 2002: International Conference Amsterdam, The Netherlands, April 21-24, 2002 Proceedings, Part III, pages 632–641. Berlin, Heidelberg: Springer Berlin Heidelberg, 2002.
- [77] D. M. Barnett. The displacement field of a triangular dislocation loop. Philosophical Magazine A, 51(3):383–387, 1985.
- [78] Hyung Jun Chang, Marc Fivel, David Rodney, and Marc Verdier. Simulations multi-échelles de l’indentation de métaux CFC: De l’atome au milieu continu. Comptes Rendus Physique, 11(3-4):285–292, 2010.
- [79] A. Hartmaier, M. C. Fivel, G. R. Canova, and P. Gumbsch. Image stresses in a free-standing thin film. Modelling and Simulation in Materials Science and Engineering, 7(5):781–793, 1999.
- [80] Caizhi Zhou, S Bulent Biner, and Richard LeSar. Discrete dislocation dynamics simulations of plasticity at small scales. Acta Materialia, 58(5):1565–1577, 2010.
- [81] O.C. Zienkiewicz, R.L. Taylor, and J.Z. Zhu, editors. The Finite Element Method: Its Basis and Fundamentals. Butterworth-Heinemann, Oxford, seventh edition edition, 2013.
- [82] M Fivel, C Robertson, G Canova, and L Boulanger. Three-dimensional modeling of indent-induced plastic zone at a mesoscale. Acta Materialia, 46(17):6183 – 6194, 1998.
- [83] Shyamal Roy and Dan Mordehai. Annihilation of edge dislocation loops via climb during nanoindentation. Acta Materialia, 127:351 – 358, 04 2017.
- [84] Qing-Jie Li, Bin Xu, Shotaro Hara, J Li, and Evan Ma. Sample-size-dependent surface dislocation nucleation in nanoscale crystals. Acta Materialia, 145:19 – 29, 02 2018.
- [85] Jonathan Amodeo, Emile Maras, and David Rodney. Site dependence of surface dislocation nucleation in ceramic nanoparticles. npj Computational Materials, 7(1):60, 2021.
- [86] Stav Nisany and Dan Mordehai. A Multiple Site Type Nucleation Model and Its Application to the Probabilistic Strength of Pd Nanowires. Metals, 12(2):280, 2022.
- [87] Christophe Geuzaine and Jean-François Remacle. Gmsh: A 3-d finite element mesh generator with built-in pre-and post-processing facilities. International journal for numerical methods in engineering, 79(11):1309–1331, 2009.
- [88] Minsheng Huang, Shuang Liang, and Zhenhuan Li. An extended 3D discrete-continuous model and its application on single- and bi-crystal micropillars. Modelling and Simulation in Materials Science and Engineering, 25(3):1 – 35, 02 2017.
- [89] T. Mura. Continuous distribution of moving dislocations. Philosophical Magazine, 8(89):843–857, 1963.
- [90] T. J. Gosling and J. R. Willis. A line-integral representation for the stresses due to an arbitrary dislocation in an isotropic half-space. Journal of the Mechanics and Physics of Solids, 42(8):1199–1221, 1994.
- [91] S Queyreau, J Marian, BD Wirth, and A Arsenlis. Analytical integration of the forces induced by dislocations on a surface element. Modelling and Simulation in Materials Science and Engineering, 22(3):035004, 2014.

- [92] Sylvain Queyreau, Khiem Hoang, Xiangjun Shi, Sylvie Aubry, and Athanasios Arsenlis. Analytical integration of the tractions induced by non-singular dislocations on an arbitrary shaped triangular quadratic element. Modelling and Simulation in Materials Science and Engineering, 28(7):075001, 2020.
- [93] T El-Achkar and D Weygand. Aspects on numerical integration of dislocation surface traction fields for discrete dislocation dynamics fem coupling: the case of emerging dislocations. Modelling and Simulation in Materials Science and Engineering, 28(8):085010, 2020.